

A Novel Model for Layer Jamming-based Continuum Robots

Bowen Yi[†], Yeman Fan[†], and Dikai Liu

Abstract—Continuum robots with variable stiffness have gained wide popularity in the last decade. Layer jamming (LJ) has emerged as a simple and efficient technique to achieve tunable stiffness for continuum robots. Despite its merits, the development of a control-oriented dynamical model tailored for this specific class of robots remains an open problem in the literature. This paper aims to present the first solution, to the best of our knowledge, to close the gap. We propose an energy-based model that is integrated with the LuGre frictional model for LJ-based continuum robots. Then, we take a comprehensive theoretical analysis for this model, focusing on two fundamental characteristics of LJ-based continuum robots: shape locking and adjustable stiffness. To validate the modeling approach and theoretical results, a series of experiments using our *OctRobot-1* continuum robotic platform was conducted. The results show that the proposed model is capable of interpreting and predicting the dynamical behaviors in LJ-based continuum robots.

I. INTRODUCTION

Continuum robots can be used in many applications due to their inherent flexibility and light weight. When interacting with the environment or humans, there is a need to actively change the dynamical response of the robots, particularly mechanical impedance. Indeed, numerous continuum robots have integrated variable stiffness techniques within their design, allowing for flexible soft motion or rigid resistance and greatly expanding their range of applications [4, 16].

Among various stiffening techniques, jamming approaches have shown great success in adjustable stiffness continuum robots with rapid reversible responses [5, 15, 19]. They can be broadly classified into fiber, granular, and layer jamming. Notably, layer jamming (LJ), the concept of which was originally proposed in [12, 13], has received particular attention due to light weight and compactness. It utilizes thin plastic or paper layers as its jamming flaps. For LJ-based continuum robots, there is an airtight pneumatic chamber in which a series of overlapping layers are installed to cover the robot spine or wrapped as the robot body. This mechanism exploits the friction between layers that can be controlled by external pressure via a vacuum, and provides a large range of controllable stiffness.

Feedback control is one of the most important topics in the field of continuum robotics, though still in infancy. Over the past few years, *model-based* approaches have gained

This work was supported in part by the Australian Research Council (ARC) Discovery Project under Grant DP200102497, and by the Robotics Institute, University of Technology Sydney, Australia.

The authors are with the Robotics Institute, University of Technology Sydney, NSW 2007, Australia. Email: {bowen.yi, dikai.liu}@uts.edu.au, yeman.fan@student.uts.edu.au.

[†]B. Yi and Y. Fan contributed equally to this work. (*Corresponding author: Y. Fan*)

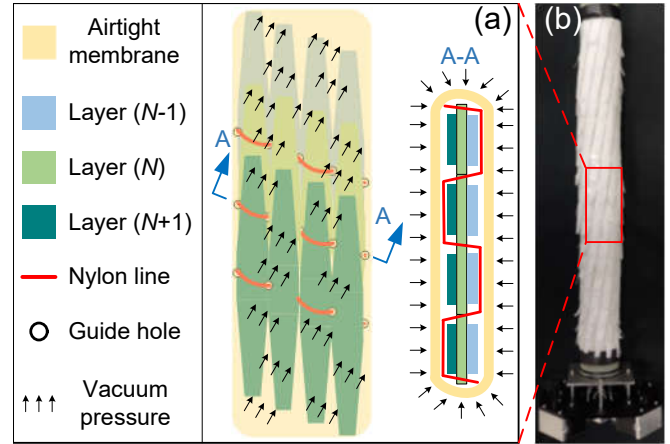


Fig. 1. Schematic of a layer-jamming structure in continuum robots

resurgence since more experimental evidence has shown that feedback approaches are robust to approximations for continuum robot dynamics [7, 9]. However, as figured out in [17], the modeling of LJ-based continuum robots with variable stiffness has not been well addressed yet. There are some recent works on analytical or computational models to characterize the mechanism of stiffness variation in LJ-based continuum robots [13, 17, 22]. However, to the best of the authors' knowledge, there is no *control-oriented* model in the literature that approximates their dynamical behaviors.

In this paper, we aim to close the above-mentioned gap by proposing a novel model for a class of LJ-based, tendon-driven continuum robots. It integrates the energy-based modeling technique and the LuGre frictional model [1]. The overall model is in port-Hamiltonian form with the vacuum pressure gradient as an additional control input. We theoretically prove the model's ability to illustrate the important phenomena of shape locking and adjustable stiffness. Besides, we present an analytical relation between stiffness and negative pressure.

Notation. All functions and mappings are assumed to be C^2 -continuous. I_n is the $n \times n$ identity matrix, $0_{n \times s}$ is an $n \times s$ matrix of zeros, and $\mathbf{1}_n := \text{col}(1, \dots, 1) \in \mathbb{R}^n$. For $x \in \mathbb{R}^n$, $S \in \mathbb{R}^{n \times n}$, $S = S^T > 0$, we denote the Euclidean norm $\|x\|^2 := x^T x$, and the weighted-norm $\|x\|_S^2 := x^T S x$. Given a function $f : \mathbb{R}^n \rightarrow \mathbb{R}$, we define the differential operators $\nabla f := (\frac{\partial f}{\partial x})^T$, $\nabla_{x_i} f := (\frac{\partial f}{\partial x_i})^T$, where $x_i \in \mathbb{R}^p$ is an element of the vector x . The set \bar{n} is defined as $\bar{n} := \{1, \dots, n\}$. We use $\text{diag}\{x_i\}$ ($i \in \bar{n}$) to represent the diagonal matrix $\text{diag}\{x_1, \dots, x_n\}$, and define the set $B_\varepsilon(\mathcal{X}) := \{x \in \mathbb{R}^n : \inf_{y \in \mathcal{X}} \|x - y\| \leq \varepsilon\}$ for a given

set $\mathcal{X} \in \mathbb{R}^n$. When clear from the context, the arguments of the functions may be omitted.

II. DYNAMIC MODELING

A. Preliminary of Jamming-free Model

In our previous work [21], we consider the control-oriented modeling of a class of underactuated tendon-driven continuum robots. A high-dimensional rigid link model is used to approximate the dynamical behavior of continuum robots as follows:

$$\begin{bmatrix} \dot{q} \\ \dot{p} \end{bmatrix} = \begin{bmatrix} 0_{n \times n} & I_n \\ -I_n & -D(q) \end{bmatrix} \begin{bmatrix} \nabla_q H \\ \nabla_p H \end{bmatrix} + \begin{bmatrix} 0_n \\ G(q)u \end{bmatrix} \quad (1)$$

with the configuration variable $q \in \mathcal{X} \subset \mathbb{R}^n$, the generalized momentum $p \in \mathbb{R}^n$, the input matrix $G : \mathbb{R}^n \rightarrow \mathbb{R}^{n \times m}$, the damping matrix $D(q) \in \mathbb{R}_{\geq 0}^{n \times n}$, and the tension input $u \in \mathbb{R}^m$. The total energy is characterized by the Hamiltonian as

$$H(q, p) = \frac{1}{2} p^\top M^{-1}(q) p + U(q), \quad (2)$$

where $M : \mathbb{R}^n \rightarrow \mathbb{R}_{>0}^{n \times n}$ is the positive definite inertial matrix satisfying $m_1 I \preceq M(q) \preceq m_2 I$ for some $m_2 \geq m_1 > 0$, and the potential energy function $U(q)$ contains the gravitational part U_G and the elastic part U_E that are functions of q , i.e.

$$U(q) = U_G(q) + U_E(q). \quad (3)$$

It is shown in [21] that these functions can be modeled as

$$\begin{aligned} U_G &= \alpha_1 [1 - \cos(q_\Sigma)] \\ U_E &= \frac{1}{2} q^\top \Lambda q + U_0 \end{aligned} \quad (4)$$

with the diagonal matrix $\Lambda := \text{diag}\{\alpha_2, \dots, \alpha_2\}$, some positive scalar U_0 and $q_\Sigma := \sum_{i \in \bar{n}} q_i$. Note that α_1 and α_2 are some elastic and gravitational coefficients, respectively. We refer the interested reader to [21] for more details about the robotic structure and its modeling procedure.

B. Friction Model for Layer Jamming

In continuum robots, the layer jamming technique provides a lightweight and rapid response approach to adjust the robots' stiffness [3, 10, 17]. In these robots, layer jamming – consisting of a laminate of flexible strips or sheets – is installed throughout the continuum robot's body, and wound up into a tube sheath, as illustrated in Fig. 1. In [21], the robot is operated in the mode that behaves highly compliant. Meanwhile, the jamming sheath forms an enclosed structure in which we may apply a negative pressure $-u_p \leq 0$ (relative to the atmospheric pressure) [8]. As a result, friction between strips or sheets would increase dramatically, thus changing the robot stiffness and dissipating energy [17].

As described above, the pressure value $u_p \in \mathbb{R}_{\geq 0}$ can be adjusted online and viewed as an additional input that changes the robotic dynamics. One of the main objectives of this paper is to propose a control-oriented dynamical model for LJ-based continuum robots. For control purposes, it is useful to have simple models that describe the essential properties of continuum robots with layer jamming; in particular,

when the pressure $u_p = 0$, the model to be obtained should degrade into the LJ-free model in Section II-A.

First, we discuss the dependence of the plant parameters α_i ($i = 1, 2$) and the function $D(q)$ on u_p . We make the following assumptions.

Assumption 1: During the variation process of u_p , the continuum robot satisfies

- (a) The mass change of air in the airtight membrane is negligible. Hence, the gravitational parameter α_1 is constant and thus *independent* of the pressure u_p .
- (b) The elastic coefficient $\alpha_2 > 0$ is constant.

Assumption 2: The energy dissipation of the robot is only derived from the lumped friction torque with $D(q) = 0$.

Under the above assumptions, the model (1) of the LJ-based continuum robot can be compactly written as

$$\Sigma_r : \begin{cases} \dot{x} = J \nabla H(x) + G_r(x)u - G_f \tau_f \\ v = G_f^\top \nabla H(x) \end{cases} \quad (5)$$

with the new variable $x := \text{col}(q, p)$ and

$$\begin{aligned} G_r &:= \begin{bmatrix} 0_{n \times m} \\ G(q) \end{bmatrix}, \\ G_f &:= \begin{bmatrix} 0_{n \times n} \\ I_n \end{bmatrix}, \\ J &:= \begin{bmatrix} 0_{n \times n} & I_n \\ -I_n & 0_{n \times n} \end{bmatrix}, \end{aligned}$$

where $\tau_f \in \mathbb{R}^n$ is the lumped frictional torque acting in the links. If we view the friction τ_f as the ‘‘input’’, then the *passive output* $v \in \mathbb{R}^n$ is, indeed, the generalized velocity [18, 20], i.e.,

$$v = M^{-1}(q)p. \quad (6)$$

The jamming phenomenon is due to the distributed friction along the layers, and the remaining task boils down to studying the modeling of the frictional effects from τ_f and its interconnection to the system Σ_r .

To take this behavior into account in the model, we consider the LuGre friction model which was proposed in [6]. It is a *dynamical* model capable of describing many frictional properties, such as zero slip displacement (a.k.a. micromotion), slick-slip motion, invariance, state boundedness, and passivity [1].

Before presenting the LuGre model, we make the following assumption about the (lumped) normal force $F_n > 0$ between the surfaces.

Assumption 3: The pressure along the layer is uniformly distributed with the value $(-u_p)$ and is proportional to the lumped normal force, i.e., $F_n \propto u_p$.

To facilitate the following analysis, we adopt the port-Hamiltonian form of the LuGre model [14]:

$$\Sigma_z : \begin{cases} \dot{z} = -R_z(v) \nabla H_z(z) + [\mathcal{N}(v) - \mathcal{P}(v)]v \\ \tau_f = [\mathcal{N}(v) + \mathcal{P}(v)]^\top \nabla H_z(z) + S v, \end{cases} \quad (7)$$

where $z \in \mathbb{R}^n$ represents the virtual bristle deflection at each joint, $v \in \mathbb{R}^n$ is the input – the relative generalized velocity of the surfaces in contact given by (6), and the output $\tau_f \in$

\mathbb{R}^n is the frictional torque. The mappings in Σ_z include the virtual bristle potential energy

$$H_z(z) = \frac{1}{2}\sigma_0 u_p |z|^2, \quad (8)$$

the damping matrix

$$\begin{aligned} R_z(v) &= \text{diag}(\beta_1(v), \dots, \beta_n(v)) \\ \beta_i(v) &:= \frac{|v_i|}{u_p \rho(v_i)}, \quad i \in \bar{n} \end{aligned} \quad (9)$$

the state-modulation matrices

$$\begin{aligned} \mathcal{N}(v) &:= I_n - \frac{1}{2}\sigma_1 u_p R_z(v) \\ \mathcal{P}(v) &:= -\frac{1}{2}\sigma_1 u_p R_z(v) \\ S &:= (\sigma_1 + \sigma_2) u_p I_n, \end{aligned} \quad (10)$$

and the function

$$\rho(v_i) = \mu_C + (\mu_S - \mu_C) \exp\left(-\left|\frac{v_i}{v_s}\right|^{\sigma_3}\right). \quad (11)$$

Physical meanings of coefficients in the above model are summarized in Table I. The interested reader may refer to [2, 6, 14] for additional details.

TABLE I
LIST OF COEFFICIENTS IN THE LUGRE MODEL

| | |
|------------|--|
| μ_S | Stiction friction coefficient |
| μ_C | Coulomb friction |
| v_s | Stribeck velocity |
| σ_0 | Bristle stiffness coefficient |
| σ_1 | Bristle damping coefficient |
| σ_2 | Viscous friction coefficient |
| σ_3 | Curve parameter (further tuning of the Stribeck effects) |

Remark 1: The model Σ_z is well-posed for all $u_p \geq 0$ even though u_p appears in the denominator of the function β_i in (9). There is due to the product $R_z(v)\nabla H_z$ in the dynamics and ∇H_z being linear in u_p . If the pressure $u_p = 0$, we have $\tau_f = 0$ for which we roughly regard zero friction injected to the robotic mechanical dynamics Σ_r . The friction torque τ_f at the steady-state stage becomes $\tau_f^{\text{ss}} = [\text{diag}\{\rho(v_i)\}\text{sign}(v) + \sigma_2 v]u_p$, with $\text{sign}(v) := \text{col}(\text{sign}(v_1), \dots, \text{sign}(v_n))$ collecting the signs of v_i .

Remark 2: The LuGre model has the boundedness property for the internal state, i.e., the set $\mathcal{E}_z := \{z \in \mathbb{R}^n : |z| \leq \frac{\mu_S}{\sigma_0}\}$ [1]. The input-output pair (v, τ_f) satisfies the particularly appealing passivity property

$$\int_0^t v^\top(s) \tau_f(s) ds \geq H_z(z(t)) - H_z(z(0)), \quad \forall t \geq 0$$

if the coefficients satisfy some inequality constraints [2].

C. Variable Stiffness Model with Layer Jamming

The overall dynamical model for the LJ-based continuum robots is the negative interconnection of Σ_r and Σ_z . For convenience, we define the full systems state as

$$\chi := \text{col}(q, p, z) \in \mathbb{R}^{3n}. \quad (12)$$

Its dynamics can be compactly written in port-Hamiltonian form as [14]

$$\dot{\chi} = [\mathcal{J} - \mathcal{R}]\nabla \mathcal{H} + \mathcal{G}(\chi)u \quad (13)$$

with the total Hamiltonian

$$\begin{aligned} \mathcal{H}(\chi, u_p) &:= H(q, p) + H_z(z, u_p) \\ &= \underbrace{\frac{1}{2}p^\top M^{-1}(q)p}_{\text{kinematic energy}} + \underbrace{\frac{1}{2}\sigma_0 u_p |z|^2 + U(q)}_{\text{potential energy}} \end{aligned} \quad (14)$$

and the matrices

$$\begin{aligned} \mathcal{J}(\chi, u_p) &:= \begin{bmatrix} J & -G_f \mathcal{N}^\top \\ \mathcal{N} G_f^\top & 0_{n \times n} \end{bmatrix} \\ \mathcal{R}(\chi, u_p) &:= \begin{bmatrix} G_f S(v) G_f^\top & G_f \mathcal{P}^\top \\ \mathcal{P}^\top G_f^\top & R_z \end{bmatrix} \\ \mathcal{G}(\chi) &:= [G_r^\top \quad 0_{n \times m}^\top]^\top. \end{aligned} \quad (15)$$

Note that \mathcal{N}, \mathcal{P} and S are linear functions of the pressure u_p . The overall model has an $(m+1)$ -dimensional input

$$u_\chi = \begin{bmatrix} u \\ u_p \end{bmatrix}$$

with all the elements non-negative.

Remark 3: The damping matrix \mathcal{R} can be expanded as $\mathcal{R} = \text{diag}(0_{n \times n}, \mathcal{R}_{22})$ with

$$\mathcal{R}_{22} := \begin{bmatrix} (\sigma_1 + \sigma_2) u_p I_n & -\frac{1}{2} \sigma_1 u_p R_z(v) \\ -\frac{1}{2} \sigma_1 u_p R_z^\top(v) & R_z(v) \end{bmatrix}.$$

Clearly, the positive semidefiniteness of \mathcal{R} is equivalent to

$$\sigma_1 + \sigma_2 - \frac{|v_i|}{4\rho(v_i)} \geq 0, \quad i \in \bar{n}. \quad (16)$$

For any coefficient, a small $|v|$ can always guarantee (16), thus making \mathcal{R} qualified as a *damping* matrix.

III. INTERPRETATION TO KEY PHENOMENA

In this section, we theoretically verify that the model proposed in Section II-C can interpret the two phenomena in LJ-based continuum robots – shape locking and tunable stiffness.

A. Shape Locking

Shape locking is one of the important capabilities of LJ structures when applied to continuum robots [17, 19, 22]. Tensions along the cables can change the robot's configuration from its undeformed shape; when a vacuum with negative pressure ($-u_p$) is applied before the release of tension actuation, the continuum robot is able to preserve its current shape. This phenomenon is known as shape locking. In this subsection, we aim to illustrate that shape locking can be characterized by the proposed model. First, we formulate its mathematical definition as follows.

Definition 1: (Shape Locking) Consider the LJ-based continuum robotic model with zero input u . If the deformed

configuration $\bar{q} \neq 0_3$ guarantees the set $\mathcal{E}_{\text{SL}} := \{(q, p, z) \in \mathbb{R}^{3n} : q = \bar{q}, p = 0_3\}$ under $u_p > 0$ forward invariant, i.e.,

$$\chi(0) \in \mathcal{E}_{\text{SL}} \implies [\dot{q}(t) = 0, \dot{p}(t) = 0, \forall t \geq 0], \quad (17)$$

then we call this invariance as shape locking.

The following proposition gives a theoretical analysis of the shape-locking phenomenon using the proposed model. Immediately after its proof, we will show an intuitive illustration.

Proposition 1: Consider the LJ-based continuum robot model (13) without external input, i.e., $u = 0_m$. For arbitrary configuration $q_a \in \mathbb{R}^n$ and a constant pressure $u_p > 0$,

- (a) There exists a vector $z_a \in \mathbb{R}^n$ such that $(q_a, 0_n, z_a)$ is an equilibrium;
- (b) The equilibria manifold

$$\mathcal{M} := \{(q, p, z) \in \mathbb{R}^{3n} : p = 0, \nabla U(q) = \sigma_0 u_p z\}$$

is locally asymptotically stable.

Proof: First, let us verify the existence of z_a such that $(q_a, 0_n, z_a)$ is an equilibrium. From (6), $p = 0$ implies the velocity $v = 0$, thus

$$\dot{q} = \nabla_p H = M^{-1}(q)p = 0.$$

The dynamics of z is given by

$$\dot{z} = -R_z(0)\nabla H_z + [\mathcal{N} - \mathcal{P}]v \Big|_{v=0} = 0,$$

where we have used the fact $R_z(0) = 0$ from (9). For the momentum, we have the following:

$$\begin{aligned} \dot{p} &= -\frac{\partial}{\partial q} \left\{ \frac{1}{2} p^\top M^{-1}(q)p \right\} - \nabla U(q_a) + S v \\ &\quad + [\mathcal{N} + \mathcal{P}]\nabla H_z \Big|_{p=0} \\ &= -\nabla U(q_a) + [I_n - \sigma_1 u_p R_z(v)]\sigma_0 u_p z \\ &= -\nabla U(q_a) + \left(I_n - \sigma_1 \text{diag} \left\{ \frac{|v_i|}{\rho(v_i)} \right\} \right) \Big|_{v=0} \sigma_0 u_p z \\ &= -\nabla U(q_a) + \sigma_0 u_p z. \end{aligned} \quad (18)$$

Hence, for any non-zero u_p , the point $\chi_* := \text{col}(q_a, 0_n, z_a)$ with

$$z_a := \frac{1}{\sigma_0 u_p} \nabla U(q_a) \quad (19)$$

is an equilibrium.

The next step of the proof is to show the local asymptotic stability of the manifold \mathcal{M} . Calculating the time derivative of the overall Hamiltonian, it yields for $\chi \in B_\varepsilon(\mathcal{M})$ with a small $\varepsilon > 0$,

$$\begin{aligned} \dot{H} &= -[\nabla \mathcal{H}(\chi, u_p)]^\top \mathcal{R}(\chi, u_p) \nabla \mathcal{H}(\chi, u_p) \\ &\leq -\left\| \begin{bmatrix} \nabla_p \mathcal{H} \\ \nabla_z \mathcal{H} \end{bmatrix} \right\|_{\mathcal{R}_{22}}^2 \\ &\leq 0, \end{aligned} \quad (20)$$

in which we have used the fact that in $B_\varepsilon(\mathcal{M})$ the matrix \mathcal{R} is positive semidefinite from Remark 3. Thus, in the

neighborhood of the manifold \mathcal{M} , the system is Lyapunov stable. In the set

$$\{\chi \in \mathbb{R}^{3n} : \|\text{col}(\nabla_p \mathcal{H}, \nabla_z \mathcal{H})\|_{\mathcal{R}_{22}} = 0\}, \quad (21)$$

it should verify

$$(\sigma_1 + \sigma_2)M^{-1}(q)p - \frac{1}{2}\sigma_0\sigma_1 u_p R_z(v)z = 0 \quad (22)$$

$$-\frac{1}{2}\sigma_1 R_z(v)M^{-1}(q)p + \sigma_0 R_z(v)z = 0. \quad (23)$$

Let us first consider (23). There are two possible cases:

- case (i): $R_z(v) = 0$ (or equivalently $p = 0$).
- case (ii): For some $j \in \bar{n}$, $\beta_j(v) \neq 0$, and thus

$$M^{-1}(q)p = 2\frac{\sigma_0}{\sigma_1}z. \quad (24)$$

For case (i), the trajectory verifies $p(t) \equiv 0$, thus

$$\dot{p} = -\nabla U(q) + \sigma_0 u_p z = 0,$$

which is exactly the manifold \mathcal{M} . For case (ii), we substitute (24) into (22), resulting in

$$4(\sigma_1 + \sigma_2)z = \sigma_1^2 \beta_j(v) u_p z. \quad (25)$$

There are two sub-cases: case (ii-1) $z = 0$ and case (ii-2) $z \neq 0$. For case (ii-1), the trajectory should guarantee $z \equiv 0$ and thus

$$\begin{aligned} \dot{z} &= -\mathcal{R}_z(v)\nabla H_z(0) + [\mathcal{N} - \mathcal{P}]v \Big|_{v \neq 0} \\ &= [\mathcal{N} - \mathcal{P}]v \Big|_{v \neq 0} = 0. \end{aligned}$$

Since $\mathcal{N} - \mathcal{P} = I_n$, it contradicts with $v \neq 0$ in case (ii). Thus, there is no feasible trajectory. For case (ii-2), the equation (25) can be rewritten as

$$\sigma_1 + \sigma_2 = \sigma_1^2 \frac{|v_j|}{4\rho(v_j)}. \quad (26)$$

Note that $\lim_{|v| \rightarrow 0} \rho(v_j) = \mu_C$. For given coefficients σ_1, σ_2 , the equation (26) does not admit any feasible solution for a sufficiently small $\varepsilon > 0$. Therefore, the only feasible solutions in $B_\varepsilon(\mathcal{M})$ are all on the equilibria manifold \mathcal{M} .

The system is time invariant since we consider constant pressure u_p . As we have shown above, \mathcal{M} is the largest invariant set in the neighborhood $B_\varepsilon(\mathcal{M}) \subset \mathbb{R}^{3n}$. Applying the LaSalle's invariance principle [11, Sec. 3], the manifold \mathcal{M} is locally asymptotically stable. ■

Remark 4: The above proposition shows that

- (i) If the initial condition $\chi(0)$ starts from any configuration q_a and zero momentum $p(0) = 0$, we may always find a virtual bristle vector z_a such that the system trajectory maintains at the initial values over time, and we also note $\mathcal{M} \subset \mathcal{E}_{\text{SL}}$. In this way, it achieves shape locking.
- (ii) A more realistic scenario is that the continuum robot achieves deformation with the tension input $u \in \mathbb{R}^m$; then we apply a vacuum and release the actuator. Once the tension release is completed, the initial condition is given by $\chi(0) = (q(0), 0_3, 0_3)$ instead of $(q_a, 0_3, z_a)$.

Proposition 1(b) shows the *local* asymptotic stability of the manifold \mathcal{M} , which means if the initial distance

$$d(\chi(0), \mathcal{M}) := \inf_{\chi' \in \mathcal{M}} |\chi' - \chi(0)| < \varepsilon_0 \quad (27)$$

is small, the trajectory ultimately converges to equilibrium $(q_a, 0_3, z_a) \in \mathcal{M}$.

(iii) From (ii), the convergence only happens when $\varepsilon_0 > 0$ is small. Note that the vector z_a is parameterized as $z_a = \frac{1}{\sigma_0 u_p} \nabla U(q_a)$. Thus, a large value of u_p can impose the initial condition $(q(0), 0_3, 0_3)$ in a small neighborhood of \mathcal{M} ; see Fig. 2 for an intuitive illustration. *Physically, it means that a large pressure value u_p is capable of achieving shape locking.*

(iv) The above item shows that after releasing the actuation, the system will change from the initial configuration $(q(0), 0_3, 0_3)$ to the new equilibrium $(q_a, 0_3, z_a)$, and it will be closed to each other with a high pressure u_p . It means when the continuum robot changes from flexible to stiff, we may observe a tiny positional change that has been experimentally verified in [4, Sec. III-B].

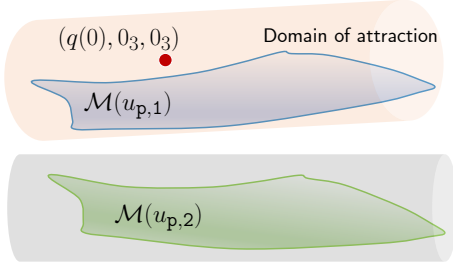


Fig. 2. An illustration of the initial condition and the equilibria manifold \mathcal{M} . For a given initial condition $(q(0), 0_3, 0_3)$, a larger $u_{p,1}$ implies a smaller distance from $\chi(0)$ to \mathcal{M} , thus $\chi(0)$ located in its domain of attraction; a smaller $u_{p,2}$ may cause the initial condition outside the domain of attraction, failing to achieve shape locking.

B. Adjustable Open-loop Stiffness

The open-loop equilibrium $\chi_* := (q_*, p_*, z_*)$ is the origin. In the stiffness analysis, we assume that there is an external torque τ_{ext} acting on the dynamics of p , i.e., the dynamics with $u = 0$ becomes

$$\dot{\chi} = [\mathcal{J} - \mathcal{R}] \nabla \mathcal{H} + G_0 \tau_{\text{ext}}. \quad (28)$$

with $G_0 = \text{col}(0_{3 \times 3}, I_3, 0_{3 \times 3})$, under which there is a shifted equilibrium $\bar{\chi} := \text{col}(\bar{q}, 0, \bar{z})$.

Definition 2: (Stiffness) Assume that we can find a positive semidefinite matrix $K \in \mathbb{R}^{3 \times 3}$ such that

$$\tau_{\text{ext}} := K(\bar{q} - q_*) \quad (29)$$

solves (28)-(29). When taking $\bar{q} \rightarrow q_*$ and $\bar{z} \rightarrow z_*$, if the limit of K exists, we call K the overall stiffness.

We are now in position to present the open-loop stiffness of the proposed LJ-based continuum robotic model.

Proposition 2: Consider the LJ-based continuum robotic model (13). Its overall stiffness in the sense of Definition 2 at the open-loop equilibrium χ_* is given by

$$K = \alpha_1 \mathbf{1}_{n \times n} + [\alpha_2 + \sigma_0 u_p] I_n, \quad (30)$$

with $\mathbf{1}_{n \times n} \in \mathbb{R}^{n \times n}$ an all elements ones.

Proof: Let us consider a tiny displacement $(\delta q, \delta z) \in \mathbb{R}^n \times \mathbb{R}^n$ around (q_*, z_*) , i.e.,

$$q = q_* + \delta q, \quad z = z_* + \delta z. \quad (31)$$

For ease of analysis, we rewrite the model in an Euler-Lagrangian form

$$\dot{M}(q) \ddot{q} + C(q, \dot{q}) \dot{q} + \nabla U(q) = \tau_{\text{ext}} - \tau_f \quad (32)$$

$$\dot{z} = -\sigma_0 \text{diag} \left\{ \frac{|\dot{q}_i|}{\rho(\dot{q}_i)} \right\} z + \dot{q}$$

$$\tau_f = (\sigma_0 z + \sigma_1 \dot{z} + \sigma_2 \dot{q}) u_p,$$

with zero initial condition, in which $C(q, \dot{q})$ is the Coriolis and Centrifugal term [18].

Linearizing the dynamics (32) around $q_* = 0, \dot{q}_* = 0$ and $z_* = 0$ and invoking (31), we obtain the model

$$M_* \delta \ddot{q} + [\sigma_1 u_p] \delta \dot{q} + [\nabla^2 U(q_*) + \sigma_0 u_p I_3] \delta q = \tau_{\text{ext}} + \mathcal{O}(\delta q^2) \quad (33)$$

with $M_* := M(q_*)$ and high-order remainder term $\mathcal{O}(\delta q^2)$, in which we have used the facts

$$C(q_*, 0) = 0, \quad \nabla U(q_*) = 0.$$

Since

$$\begin{aligned} \sigma_1 u_p &> 0 \\ \nabla^2 U(q_*) + \sigma_0 u_p I_3 &> 0, \end{aligned}$$

the linearized dynamics (33) is exponentially stable at equilibrium

$$\delta q = [\nabla^2 U(q_*) + \sigma_0 u_p I_3]^{-1} \tau_{\text{ext}} + \mathcal{O}(\delta q^2).$$

By taking $|\delta q| \rightarrow 0$, the algebraic equation (29) is obtained with K given by

$$K = \nabla^2 U(q_*) + \sigma_0 u_p I_3.$$

Substituting the function U in (3) into the above, we obtain (30) and complete the proof. \blacksquare

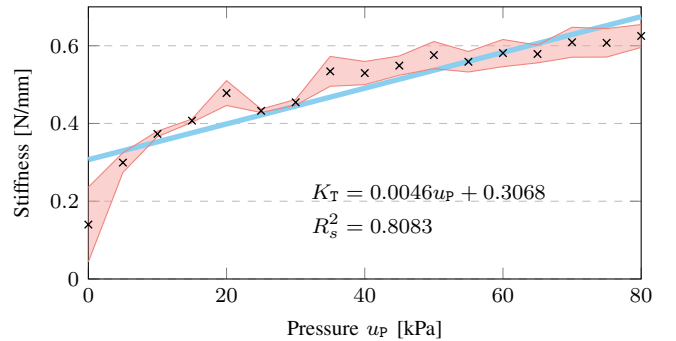


Fig. 3. Relation between u_p and the transverse stiffness from the experiments in which we used the jamming sheath with 5 layers. (“x” shows the mean values; color band represents the ± 1 standard deviation.)

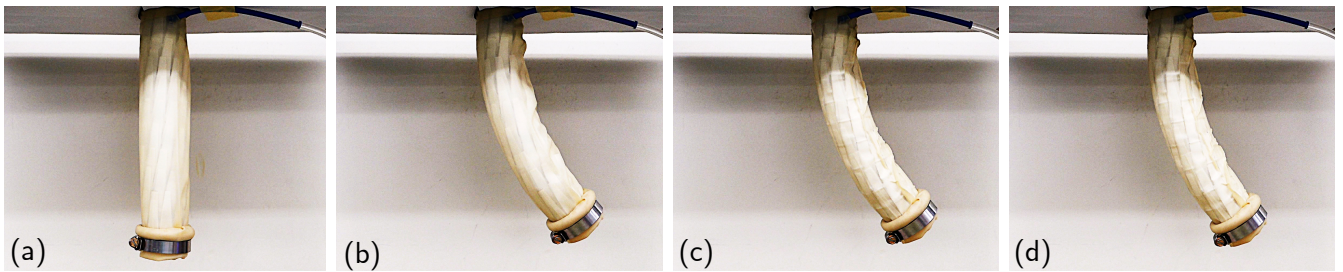


Fig. 4. Photos showing sequence of the shape-locking experiments: (a) Phase 1: Initial configuration without u ; (b) Phase 2: Drive to the bending configuration 60° via tendon force u ; (c) Phase 3: Vacuum to $u_p = 30$ kPa with motor-driven retained; (d) Phase 4: Vacuum retained and tendon released $u = 0$. (Photos were taken in the steady state of each phase.)

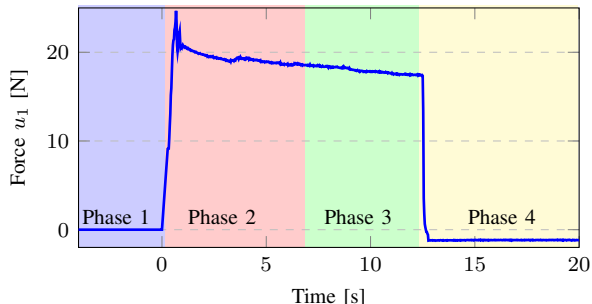


Fig. 5. Trajectory of the tendon force u_1 in the stiffness experiment.

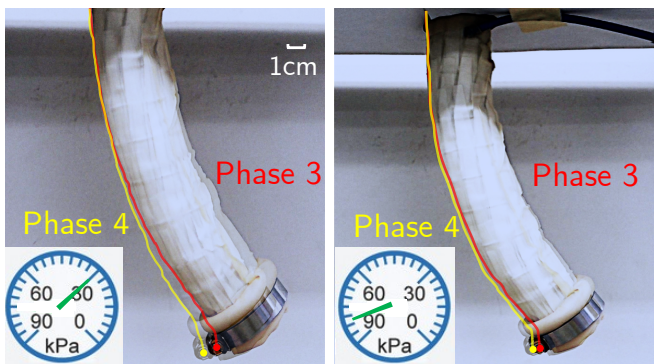


Fig. 6. Overlay photos of the shape-locking phenomenon. Left: displacement of 9.2mm with $u_p = 30$ kPa; Right: displacement of 3.8mm with $u_p = 80$ kPa. (“●” and “●”) are used to mark a fixed point on the robot body; one-side contours are also highlighted in the figure.)

IV. EXPERIMENTS

In this section, we verify the theoretical analysis in Section III on our continuum robotic platform *OctRobot-I*. Although the overall stiffness matrix $K \succ 0$ cannot be measured directly, we are able to detect the transverse stiffness $K_T \in \mathbb{R}_{\geq 0}$ in the end-effector around the open-loop equilibrium q_* of the continuum robot. We used the same testing setup and approach as in [21, Sec. VI-B], and repeated three times under the same conditions. The open-loop transverse stiffness under different negative pressures ($-u_p$) is plotted in Fig. 3. The coefficient of determination R_s^2 is 0.8083 showing good linearity with respect to the value u_p . This verifies the results in Section III-B.

The second experiment was designed to verify the results about shape-locking. The robot was initialized from the

open-loop configuration $q_* = 0$ (Phase 1), and then driven to the bending angle of 60° via tendon (Phase 2). When the system kept at the steady-state stage, we vacuumed and kept the jamming layer sheath to a negative pressure of -30 kPa (Phase 3), and then released the tendons (Phase 4). During this process, the sequence photos are presented in Fig. 4, and the force u_1 was tuned as the trajectory in Fig. 5. Note that we use the time interval $[-5, 0]$ s to denote the initial status before starting the motor drive. As illustrated in Figs. 4(c)-(d), it achieved shape locking after applying a negative pressure ($-u_p$). To clearly show the shape-locking phenomenon, Fig. 6 illustrates the overlay photos of Phases 3 and 4 with two different u_p (30 and 80 kPa). It can be observed tiny positional changes as theoretically predicted in Remark 4(iv) – a larger u_p yielded a smaller displacement (3.8mm of 80 kPa and 9.2mm of 30 kPa).

V. CONCLUSION

In this paper, we have presented a novel dynamical model for layer jamming-based continuum robots, which integrates the energy-based modeling approach and the LuGre frictional model. In terms of the proposed model, we theoretically analyze its dynamical behavior and show its usefulness in interpreting the two important phenomena (i.e., shape locking and adjustable stiffness) in this kind of robots with quantitative results. These have been experimental verified on our robotic platform.

The motivation of this work is to propose a *control-oriented* model, and naturally our future work will center on feedback controller synthesis using the proposed model. Another important direction is to revisit Assumption 3 regarding the relation between the pressure and lumped normal force. This would be helpful to improve the fitting accuracy on the relation between robot stiffness and negative pressure.

REFERENCES

- [1] K. J. Aström and C. Canudas-De-Wit. Revisiting the LuGre friction model. *IEEE Control Syst. Mag.*, 28(6):101–114, 2008.
- [2] N. Barahonov and R. Ortega. Necessary and sufficient conditions for passivity of the LuGre friction model. *IEEE Trans. Autom. Control*, 45(4):830–832, 2000.
- [3] W. H. Choi, S. Kim, D. Lee, and D. Shin. Soft, multi-DoF, variable stiffness mechanism using layer jamming for wearable robots. *IEEE Robot. Autom. Lett.*, 4(3):2539–2546, 2019.
- [4] A. B. Clark and N. Rojas. Assessing the performance of variable stiffness continuum structures of large diameter. *IEEE Robot. Autom. Lett.*, 4(3):2455–2462, 2019.

- [5] A. B. Clark and N. Rojas. Malleable robots: Reconfigurable robotic arms with continuum links of variable stiffness. *IEEE Trans. Robot.*, 38(6):3832–3849, 2022.
- [6] C. C. De Wit, H. Olsson, K. J. Astrom, and P. Lischinsky. A new model for control of systems with friction. *IEEE Trans. Autom. Control*, 40(3):419–425, 1995.
- [7] C. Della Santina, C. Duriez, and D. Rus. Model-based control of soft robots: A survey of the state of the art and open challenges. *IEEE Control Syst. Mag.*, 43(3):30–65, 2023.
- [8] Y. Fan, D. Liu, and L. Ye. A novel continuum robot with stiffness variation capability using layer jamming: Design, modeling, and validation. *IEEE Access*, 10:130253–130263, 2022.
- [9] E. Franco and A. Garriga-Casanovas. Energy-shaping control of soft continuum manipulators with in-plane disturbances. *Int. J. Robot. Res.*, 40(1):236–255, 2021.
- [10] S. Jadhav, M. R. A. Majit, B. Shih, J. P. Schulze, and M. T. Tolley. Variable stiffness devices using fiber jamming for application in soft robotics and wearable haptics. *Soft Robot.*, 9(1):173–186, 2022.
- [11] H. K. Khalil. *Nonlinear Systems*. Prentice Hall, 3 edition, 2001.
- [12] Y.-J. Kim, S. Cheng, S. Kim, and K. Iagnemma. Design of a tubular snake-like manipulator with stiffening capability by layer jamming. In *IEEE Int. Conf. Intell. Robots Syst.*, pages 4251–4256. IEEE, 2012.
- [13] Y.-J. Kim, S. Cheng, S. Kim, and K. Iagnemma. A novel layer jamming mechanism with tunable stiffness capability for minimally invasive surgery. *IEEE Trans. Robot.*, 29(4):1031–1042, 2013.
- [14] J. Koopman, D. Jeltsema, and M. Verhaegen. Port-Hamiltonian description and analysis of the LuGre friction model. *Simul. Model. Pract. Theory.*, 19(3):959–968, 2011.
- [15] M. Langer, E. Amanov, and J. Burgner-Kahrs. Stiffening sheaths for continuum robots. *Soft Robot.*, 5(3):291–303, 2018.
- [16] Y. S. Narang, A. Degirmenci, J. J. Vlassak, and R. D. Howe. Transforming the dynamic response of robotic structures and systems through laminar jamming. *IEEE Robot. Autom. Lett.*, 3(2):688–695, 2017.
- [17] Y. S. Narang, J. J. Vlassak, and R. D. Howe. Mechanically versatile soft machines through laminar jamming. *Adv. Funct. Mater.*, 28(17):1–9, 2018. Art. no. 1707136.
- [18] R. Ortega, A. Loria, P. J. Nicklasson, and H. Sira-Ramirez. *Passivity-based Control of Euler-Lagrange Systems: Mechanical, Electrical and Electromechanical Applications*. Springer, 1998.
- [19] J. L. C. Santiago, I. S. Godage, P. Gonthina, and I. D. Walker. Soft robots and kangaroo tails: Modulating compliance in continuum structures through mechanical layer jamming. *Soft Robot.*, 3(2):54–63, 2016.
- [20] A. van der Schaft. *L₂-Gain and Passivity Techniques in Nonlinear Control*. Springer, 3rd edition, 2017.
- [21] B. Yi, Y. Fan, D. Liu, and J. G. Romero. Simultaneous position-and-stiffness control of underactuated antagonistic tendon-driven continuum robots. *ArXiv Preprint*, 2023. (arXiv:2306.03865).
- [22] Y. Zhao *et al.* A soft continuum robot, with a large variable-stiffness range, based on jamming. *Bioinspir. Biomim.*, 14(6), 2019. Art. no. 066007.